Observations of the Effect of Ionization-Potential Depression in Hot Dense Plasma

D. J. Hoarty,[1] P. Allan,[1] S. F. James,[1] C. R. D. Brown,[1] L. M. R. Hobbs,[1] M. P. Hill,[1] J. W. O. Harris,[1] J. Morton,[1] M. G. Brookes,[1] R. Shepherd,[2] J. Dunn,[2] H. Chen,[2] E. Von Marley,[2] P. Beiersdorfer,[2] H. K. Chung,[3] R. W. Lee,[4] G. Brown,[3] and J. Emig[3]

[1]*Directorate of Research and Applied Science, AWE plc, Reading RG7 4PR, United Kingdom*
[2]*Lawrence Livermore National Laboratory, 7000 East Avenue, Livermore, California 94550, USA*
[3]*Nuclear Data Section, Division of Physical and Chemical Sciences, International Atomic Energy Agency, P. O. Box 100, A-1400 Vienna, Austria*
[4]*Institute for Material Dynamics at Extreme Conditions, University of California, Berkeley, California 94720, USA*

(Received 28 January 2013; published 26 June 2013)

The newly commissioned Orion laser system has been used to study dense plasmas created by a combination of short pulse laser heating and compression by laser driven shocks. Thus the plasma density was systematically varied between 1 and 10 g/cc by using aluminum samples buried in plastic foils or diamond sheets. The aluminum was heated to electron temperatures between 500 and 700 eV allowing the plasma conditions to be diagnosed by K-shell emission spectroscopy. The K-shell spectra show the effect of the ionization potential depression as a function of density. The data are compared to simulated spectra which account for the change in the ionization potential by the commonly used Stewart and Pyatt prescription and an alternative due to Ecker and Kröll suggested by recent x-ray free-electron laser experiments. The experimental data are in closer agreement with simulations using the model of Stewart and Pyatt.

DOI: 10.1103/PhysRevLett.110.265003 PACS numbers: 52.25.Jm, 52.50.Jm

In high density plasmas the field from neighboring ions and free electrons lowers the electron binding energies in the ions relative to the isolated ion values. Recent developments in x-ray free electron lasers have allowed the effect of ionization potential depression (IPD) to be measured in solid density aluminum. In a set of experiments at the Linac Coherent Light Source [1] edge shifts inferred from K_α fluorescence spectra were found to be in disagreement with the Stewart and Pyatt (SP) [2] IPD model widely used since the 1960s, but were closer to an even earlier IPD model proposed by Ecker and Kröll (EK) [3] as discussed in [1,4]. This has important implications for dense plasma physics and in particular for the detailed prediction of the dense plasma equation of state and radiative opacity in stellar interiors, inertial confinement fusion research, and planetary interiors where the SP model has been used widely. Ionization potential depression is difficult to measure directly because it is in general indistinguishable from the effect of the line merging of high series spectral lines by Stark broadening [5]. However, in the data presented in this work the K shell transitions from $n = 2$ and $n = 3$ initial states can be used to compare IPD models where these models predict the disappearance of lines well before they are subject to broadening sufficient to merge them. In this case there is not an ambiguity between merged bound states and those which disappear due to IPD. This Letter describes a study of the effect of IPD in plasmas heated by short pulse laser induced currents to electron temperatures between 500 and 700 eV on a time scale of a picosecond. The experiments were carried out at the newly commissioned Orion laser in the UK [6]. The experiments differ substantially from earlier work [7–10] in that these data present a study of the effect of IPD at higher energy density with the sample density varied systematically over an order of magnitude between 1–10 g/cc. This was possible because of some unique features of the Orion laser system which combines short pulse (picosecond) and long pulse (nanosecond time scale) pulses to compress and heat the sample, and by use of samples buried in plastic foils and diamond sheets. The Orion short pulse laser can operate at second harmonic wavelength which suppresses the prepulse inherent in conventional infrared laser systems and greatly increases energy coupling to the solid target [11] allowing the necessary volume of dense material to be efficiently heated. The contrast measurements carried out so far for second harmonic operation have shown the contrast is 10^{14} up to at least 100 ps before the main pulse [12]. The findings of the study are that comparing experimental measurements to spectroscopic simulations using the EK model reveals a clear overestimate of IPD with this model under the experimental conditions, but simulations using with the SP model of IPD are much closer to experimental observation.

The plastic tamped samples used in the study were aluminum dots 100 μm in diameter and 0.15 μm thick buried in a CH plastic foil (parylene-N) sandwich of 10 μm on one side and 12 μm on the other, mounted as described in Ref. [11]. The face with 10 μm coating was irradiated with beam line 1 of the Orion short pulse OPCPA laser delivering 100 J of 2ω light (0.53 μm wavelength),

converted with a type I KDP crystal, in a pulse length of 0.5 ps FWHM. The focal spot was 50 μm giving an irradiance of 1×10^{19} W/cm^2. Spectra were recorded both time resolved using an ultrafast x-ray streak camera [11] with picosecond temporal resolution coupled to a convex curved (500 mm radius of curvature) CsAP crystal and time integrated using flat and convex curved crystal spectrometers recording onto image plate. The spectral resolution ($E/\Delta E$) was 500 in the time-resolved case and 600 in the time-integrated case. The response of the spectrometers was absolutely calibrated in order to provide spectral emissivities using off-line x-ray sources to measure the image plate response and reflectivity as a function of x-ray energy.

The photocathode material used was solid caesium iodide (0.1 μm CsI/0.02 μm Al/1 μm plastic). The x-ray emission source area was measured using an x-ray pinhole array. The time integrating spectrometers were set to record spectra in the range 1.3–2.3 keV and the time-resolved spectra were recorded in the range of 1.75–2.2 keV as described in Ref. [11]. When heated by the short pulse laser the thin layer of aluminum expands into the surrounding plastic tamper but the overall foil remains at solid density for around 200 ps. The measured x-ray pulse duration is 20 ps, consistent with earlier experiments [13] and simulations. The measured spectra are compared to synthetic spectra generated by the FLY [14] and FLYCHK [15] time dependent collisional radiative models, including modeling the pulse duration. The temperature was inferred from the ratio of the Ly_β/He_β emission intensities and the density was inferred from the Stark broadened line shapes of these emission lines as reported elsewhere [11] and were 600 eV and 1.5 ± 0.5 g/cc, respectively.

To provide a controlled density variation, shocks of varied strengths were driven through the foil by irradiating the 12 μm side of the foil with two Orion long pulse beams operating in 3ω (0.36 μm wavelength) in a pulse 0.5 ns FWHM with a 140 ps rise time, 200 J in each beam and with phase plates giving uniform 300 μm focal spots. The beams were synchronized to better than 20 ps. The delay between the long pulse beams and the short pulse beam was varied in the experiments.

In the time after shock compression of the buried layer but before shock breakout, the short pulse beam irradiates the 10 μm plastic face to heat the compressed tamper and sample. Figure 1 shows the measured spectra from shock compressed aluminum in plastic. The graph shows the experimental emissivity compared to a spectrum predicted by FLYCHK with the predicted emissivity scaled by 1.17. The FLYCHK peak electron temperature was 550 eV and the density inferred was 6 g/cc. The inset curve shows the $n = 1$–3 transitions measured on the x-ray streak camera on the same laser shot as the time-integrated measurement along with a comparison to FLYCHK. The density inferred was the same as the time-integrated data but the peak

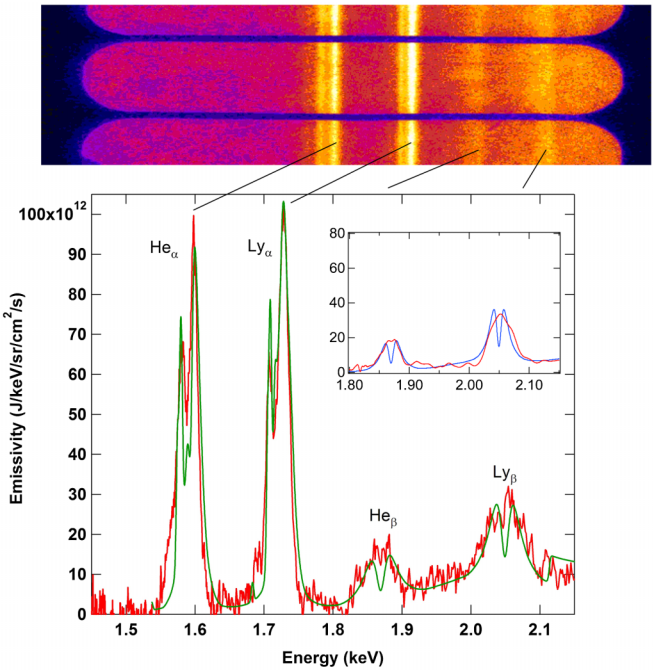

FIG. 1 (color online). Shock compressed data shown at the top and below a graph of energy vs emissivity showing a line-out through the experimental time-integrated data (red curve or dark gray) compared to a synthetic spectrum from FLYCHK (green curve or light gray). The inset curve (intensity in arbitrary units vs x-ray energy in keV) is the time resolved data recorded on the ultrafast streak camera over the range of the $n = 1$–3 transitions.

electron temperature inferred from the time-resolved data was slightly higher at 600 eV. Spectra at intermediate density, 3 g/cc and slightly higher peak electron temperature of 700 eV, were measured by using samples of aluminum tamped in diamond sheet. The targets were 100 μm diameter 0.15 μm thick aluminum dots sandwiched in 10 μm diamond at 3.5 g/cc and 4 μm diamondlike carbon at 3 g/cc. The laser conditions were identical to the plastic experiments apart from a smaller focal spot on the short pulse beam of 20 μm. The diamond tamped aluminum remains at 3 g/cc during the x-ray emission pulse. The tamping effect of the diamond is reasonably well modeled by radiation-hydrodynamics simulations using the NYM code [11,16,17].

To achieve higher densities the diamond was shocked by one of the long pulse beams of Orion incident on the 10 μm diamond face. Figure 2 shows the emission recorded on the x-ray streak camera at different delays during the transit of the shock wave through the diamond target. In the lower two curves the shock wave has not yet arrived at the aluminum dot position, and the $n = 1$–3 transitions from He-like and H-like aluminum ions are clearly visible. The delay between the onset of the long pulse and the short pulse is 200 ps and 260 ps, respectively. A comparison of the recorded spectra to FLYCHK simulations shows that the temperature is similar to that

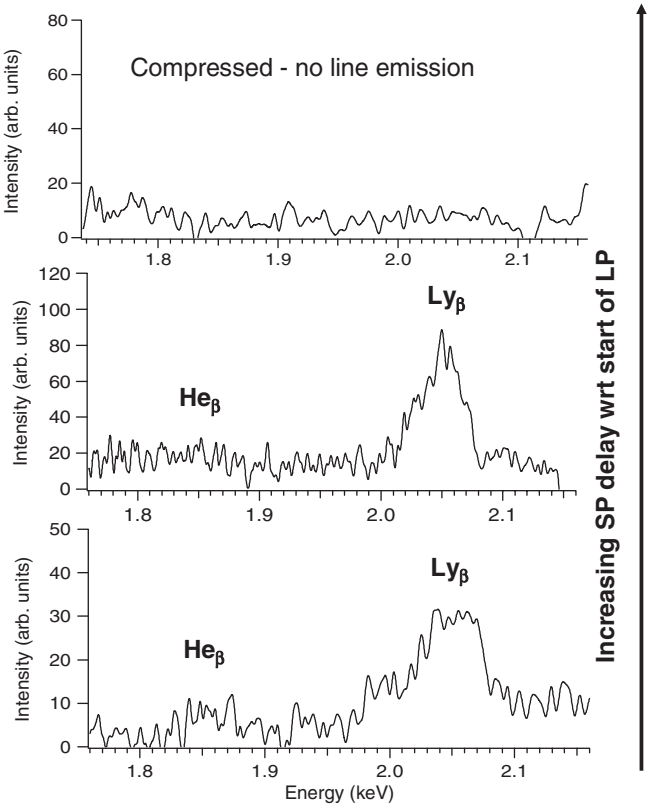

FIG. 2. Emission spectra recorded on the streak camera at various times during the shock wave transit through the target. For the bottom and middle curves the shock has not yet arrived at the aluminum layer position. In the top curve the shock has compressed the aluminum and the $n = 3$ levels have become delocalized.

recorded in the unshocked diamond experiments. In the upper curve the shock has arrived at the aluminum layer and compressed the aluminum. The $n = 3$ transitions are no longer evident in the spectrum because of the delocalization of the $n = 3$ levels in the He-like and H-like ions due to ionization potential depression. In the absence of He$_\beta$ and Ly$_\beta$ lines the conditions for the data in the top curve of Fig. 2 must be inferred from the time-integrated data. The Ly$_\alpha$ line shape was used to infer the density and the He$_\alpha$/Ly$_\alpha$ ratio was used to estimate the temperature. Though opacity effects at the line center mean that this method is not as accurate as the density and temperature inferred from the optically thin $n = 1$–3 transitions, and there is a discrepancy in the satellite line intensity, a reasonable estimate can be inferred in this case. Figure 3 shows the time-integrated spectra recorded from shock compressed aluminum in diamond. The $n = 3$ transitions are absent but the He$_\alpha$ and Ly$_\alpha$ lines can be clearly seen. The inset is a comparison of the Ly$_\alpha$ line shape with the prediction of FLYCHK which indicates a density of 9 ± 1 g/cc.

An additional estimate of the density can be taken from the radiation-hydrodynamics simulations of the shocked target. The shock transit time in the experiment was

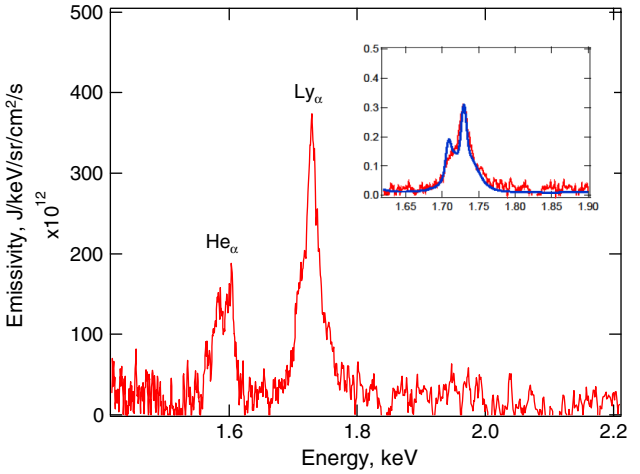

FIG. 3 (color online). X-ray emission spectra from shock compressed aluminum in diamond. Inset comparison of measured and simulated Ly$_\alpha$ line shape indicates 9 g/cc.

measured, which allowed the radiation-hydrodynamics simulations to be benchmarked. To reproduce the measured transit time in the radiation-hydrodynamics simulations the irradiance on target was reduced from the measured value. The radiation-hydrodynamics predictions for density, temperature and ionization are shown in Fig. 4. The shocked aluminum density reaches just over 10 g/cc and drops to 8 g/cc during the duration of the x-ray emission recorded on the streak camera. The predicted conditions are in reasonable agreement with those inferred from the spectra. Line-outs of the aluminum spectra measured with the ultrafast streak camera and crystal spectrometer in the range 1.8–2.2 keV are shown in Fig. 5. The measurements, at the various densities sampled experimentally, are shown alongside the predictions of the FLYCHK

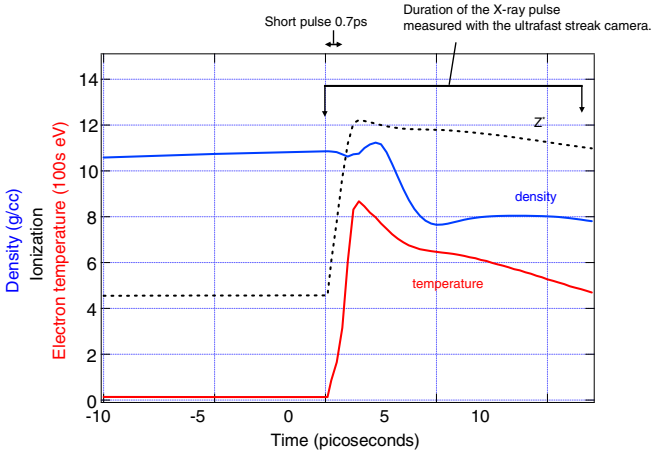

FIG. 4 (color online). Conditions in the shocked aluminum layer with a diamond tamper predicted by the radiation-hydrodynamics code. The peak electron temperature and density are in reasonable agreement with the conditions inferred from the emission spectrum.

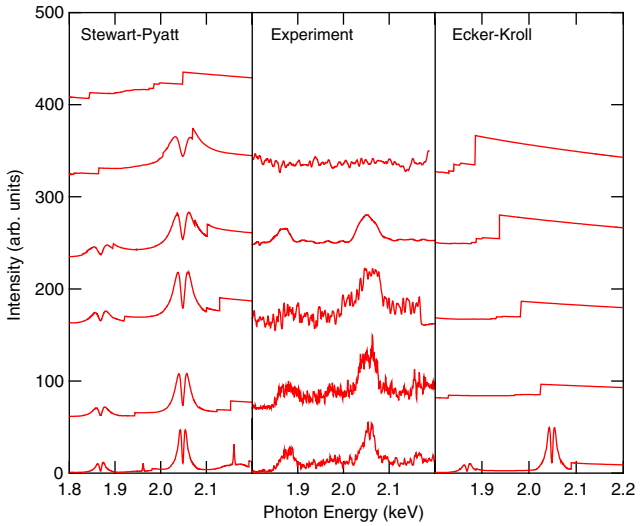

FIG. 5 (color online). A compilation of the experimental data at different densities compared to FLYCHK predictions using Stewart and Pyatt and Ecker and Kröll treatments of ionization potential depression. The density of the curves from bottom to top is 1.2, 2.5, 4, 5.5, and 9 g/cc. The SP plot has an additional curve at 11.6 g/cc.

code using both the SP and EK models of IPD, with the same prescription for SP and EK models used here as in Ref. [1]. The curves of both experiment and simulation are in arbitrary units and have been scaled in intensity for clarity. The experimental curves from bottom to top were fitted at the following conditions of the total aluminum material density and peak electron temperature: 1.2 ± 0.4 g/cc, 550 eV; 2.5 ± 0.3 g/cc, 650 eV; 4 ± 0.5 g/cc, 700 eV; 5.5 ± 0.5 g/cc, 550 eV; 9 ± 1 g/cc, 700 eV. The simulations use the measured density but the temperature in all cases is 700 eV. The simulations using the SP prescription for IPD are in qualitative agreement with experiment but suggest that delocalization of the $n = 3$ levels, from bound states to the continuum, would occur at a slightly higher density (11.6 g/cc) than indicated by the experiments. This curve is the top curve of the SP plots in Fig. 5. However the abrupt steps at the bound-free edges in the simulations are unphysical and a more realistic picture should include broadening of the bound-free edges due to fluctuations [18]. In contrast the simulations with the EK model for IPD predict a very different outcome. The EK model predicts delocalization of the $n = 3$ levels at all but the lowest density sampled in the experiment. Importantly the EK model removes the $n = 3$ level to the continuum by IPD at a density too low for Stark broadening of the lines and merging with the continuum to be an alternative possibility according to line-shape theory; a theory which has been verified against experiment over several decades [14,19–21]. The densities inferred from Stark broadening of measured spectra are consistent with the radiation-hydrodynamics predictions of the target density. On the experimental time scale the density of the tamper determines the density in the sample because the thickness of the foil or diamond sheet means there is insufficient time for the rarefaction wave from the outer surface to move inward significantly.

Following the convention in Ref. [18] in the high density limit the shift in ionization potential for SP and EK models can be written as

$$\Delta I_{\mathrm{SP}}(Z) = \frac{3(Z+1)e^2}{2R_O}, \tag{1}$$

and

$$\Delta I_{\mathrm{EK}} = \frac{(Z+1)e^2}{R_{\mathrm{EK}}}, \tag{2}$$

where

$$\frac{4\pi n_i R_o^3}{3} = 1, \tag{3}$$

and

$$R_{\mathrm{EK}}^3 = \frac{R_o^3}{1 + \langle N_e \rangle}. \tag{4}$$

Here, n_i is the ion number density, and $\langle N_e \rangle$ is the average number of free electrons per ion. For a highly ionized system ΔI_{EK} is larger than ΔI_{SP} by the additional scaling $\langle N_e \rangle^{1/3}$.

The data in Fig. 5 show that this additional shift is a large overestimate of the effect and that the Stewart and Pyatt model is closer to the experimental measurements in this regime. The data show that $n = 3$ transitions are clearly observed up to densities of at least 6 g/cc, indicating that the IPD shift has not delocalized the $n = 3$ levels. The data and radiation-hydrodynamics simulations suggest that at a density between 8 and 10 g/cc the $n = 3$ levels are delocalized and that the $n = 1$–3 line transitions disappear from the spectrum. In summary, a systematic study of the effect of IPD on the delocalization of $n = 3$ levels in aluminum has demonstrated much closer agreement between the measurements and predictions of simulations using the SP model of IPD than with those using the EK model and over the range of the experimental conditions the EK model overestimates the IPD shift significantly. Although the SP model is a simple analytical approximation relying on the semiclassical Thomas-Fermi approximation, the model prediction is close to experiment though some discrepancy remains. The data described will be compared to more sophisticated models in due course.

The authors would like to thank the laser and facility staff of the Orion laser and D. Lavender for engineering support and the staff of AWE target fabrication. Work at the Lawrence Livermore National Laboratory was performed under the auspices of the DOE under Contract No. DE-AC52-07NA-27344.

[1] O. Ciricosta *et al.*, Phys. Rev. Lett. **109**, 065002 (2012).
[2] J. C. Stewart and K. D. Pyatt, Jr., Astrophys. J. **144**, 1203 (1966).
[3] G. Ecker and W. Kröll, Phys. Fluids **6**, 62 (1963).
[4] T. R. Preston, S. M. Vinko, O. Ciricosta, H.-K. Chung, R. W. Lee, and J. S. Wark, High Energy Density Phys. **9**, 258 (2013).
[5] D. R. Inglis and E. Teller, Astrophys. J. **90**, 439 (1939).
[6] N. W. Hopps *et al.*, Proc. SPIE Int. Soc. Opt. Eng. **7916**, 79160C (2011).
[7] D. K. Bradley, J. Kilkenny, S. J. Rose, and J. D. Hares, Phys. Rev. Lett. **59**, 2995 (1987).
[8] D. Riley, O. Willi, S. J. Rose, and T. Afshar-Rad, Europhys. Lett. **10**, 135 (1989).
[9] M. Nantel, G. Ma, S. Gu, C. Côté, J. Itatani, and D. Umstadter, Phys. Rev. Lett. **80**, 4442 (1998).
[10] J. Osterholz, F. Brandl, T. Fischer, D. Hemmers, M. Cerchez, G. Pretzler, O. Willi, and S. Rose, Phys. Rev. Lett. **96**, 085002 (2006).
[11] C. R. D. Brown *et al.*, Phys. Rev. Lett. **106**, 185003 (2011).
[12] D. Hillier *et al.*, Appl. Opt. (to be published).
[13] D. J. Hoarty, S. F. James, C. R. D. Brown, B. M. Williams, H. K. Chung, J. W. O. Harris, L. Upcraft, B. J. B. Crowley, C. C. Smith, and R. W. Lee, High Energy Density Phys. **6**, 105 (2010).
[14] R. W. Lee and J. T. Larsen, J. Quant. Spectrosc. Radiat. Transfer **56**, 535 (1996).
[15] H.-K. Chung, M. H. Chen, W. L. Morgan, Y. Ralchenko, and R. W. Lee, High Energy Density Phys. **1**, 3 (2005).
[16] D. Hoarty, O. Willi, L. Barringer, C. Vickers, R. Watt, and W. Nazarov, Phys. Plasmas **6**, 2171 (1999).
[17] P. D. Roberts, S. J. Rose, P. C. Thompson, and R. J. Wright, J. Phys. D **13**, 1957 (1980).
[18] C. A. Iglesias and P. A. Sterne, High Energy Density Phys. **9**, 103 (2013).
[19] H. R. Griem, *Principles of Plasma Spectroscopy* (Cambridge University Press, Cambridge, England, 1997).
[20] H. R. Griem, *Spectral Line Broadening by Plasmas* (Academic Press, New York, 1974).
[21] H. J. Kunze, *Introduction to Plasma Spectroscopy* (Springer, New York, 2009), and references therein.